Lattice Boltzmann Modelling of Droplets on Chemically Heterogeneous Surfaces with Large Liquid-Gas Density Ratio

Yingqing ZU and Yuying YAN*

* Corresponding author: Tel.: ++44 (0) 115 951 3168; Fax: ++44 (0) 115 951 3159; Email: yuying.yan@nottingham.ac.uk
School of the Built Environment, University of Nottingham, NG7 2RD, UK

Abstract A lattice Boltzmann method which can simulate droplet dynamics on partial wetting surface with large liquid-gas density ratio is proposed. The interaction between the fluid-fluid interface and the partial wetting wall is typically considered. Using the method, the dynamics of liquid drops on chemically heterogeneous surfaces are numerically simulated. The corresponding mechanisms including droplet spreading, break-up and migration on such surfaces are studied on the basis of droplet shapes, moving contact lines and velocity fields.

Keywords: Lattice Boltzmann method, Two-phase flow, Large density ratio, Contact angle

1. Introduction

There is a large class of industrial processes which involve motions of droplets on a partial wetting surface. Operations ranging from painting, coating, inkjet printing to lubrication and gluing are a few examples. In order to perform a numerical study of such type of phenomena, lattice Boltzmann method (LBM) can be employed since, in recent years, lattice Boltzmann method has become an established numerical scheme for simulating multiphase fluid flows. The intrinsic feature enables the LBM to model phase segregation and interfacial dynamics of multiphase flow, which are difficult to be handled by applying conventional CFD methods or employing the molecular dynamics (MD) method to incorporate intermolecular interactions at mesoscopic level (Chen and Doolen, 1998).

Although some lattice Boltzmann models (Gunstensen et al., 1991; He et al., 1999; Shan and Chen, 1993; Swift et al., 1996; Swift et al., 1995) for two-phase flows on partial wetting surface have been presented, one of the disadvantages of those models is that they basically are limited to small density ratio due to numerical instability. The maximum density ratio in the simulations of droplets on partial wetting surfaces (Dupuis and Yeomans, 2004; Dupuis and Yeomans, 2005; Kusumaatmaja et al., 2006) was reported just around 2. Obviously, this is not realistic for most two-phase systems e.g. the density ratio of liquid-gas systems is usually larger than 100, and the density ratio of water to air is about 1000. Therefore, a model for large density ratio should be developed. A new LBM scheme for calculating liquid droplet behaviours on particle wetting surfaces typically for the system of liquid-gas of a large density ratio was reported by Yan and Zu (2007). In the present paper, the method is further applied to the cases of droplet in air spreading on different types of chemically heterogeneous surfaces with detailed field analysis.

2. Numerical Method

2.1. Two-phase lattice Boltzmann model

For D3Q15 LBM model, as shown in Fig. 1, the particle velocity, $\mathbf{e}_\alpha$, is given by

$$[\mathbf{e}_0,\mathbf{e}_1,\mathbf{e}_2,\mathbf{e}_3,\mathbf{e}_4,\mathbf{e}_5,\mathbf{e}_6,\mathbf{e}_7,\mathbf{e}_8,\mathbf{e}_9,\mathbf{e}_{10},\mathbf{e}_{11},\mathbf{e}_{12},\mathbf{e}_{13},\mathbf{e}_{14}] = \begin{bmatrix} 0 & 1 & 0 & 0 & -1 & 0 & 0 & 1 & -1 & 1 & 1 & -1 & 1 & -1 & -1 \\ 0 & 0 & 1 & 0 & 0 & -1 & 0 & 1 & 1 & -1 & 1 & -1 & -1 & 1 & -1 \\ 0 & 0 & 0 & 1 & 0 & 0 & -1 & 1 & 1 & 1 & -1 & -1 & -1 & -1 & 1 \end{bmatrix} \quad (1)$$

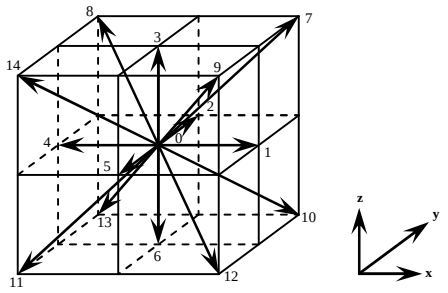

Fig. 1: D3Q15 model

To simulate a two-phase fluid flow, two particle velocity distribution functions, f_α and g_α, are introduced. Function f_α is used to calculate the order parameter, ϕ, which distinguishes the two phases. Function g_α is used to calculate the predicted velocity, $\mathbf{u}^*$, of the two-phase fluids without a pressure gradient. The evolution of the particle distribution functions $f_\alpha(\mathbf{x},t)$ and $g_\alpha(\mathbf{x},t)$ is calculated by the following equations:

$$f_\alpha(\mathbf{x}+\mathbf{e}_\alpha\delta_t, t+\delta_t) = f_\alpha^{(eq)}(\mathbf{x},t), \quad (2)$$

$$g_\alpha(\mathbf{x}+\mathbf{e}_\alpha\delta_t, t+\delta_t) = g_\alpha^{(eq)}(\mathbf{x},t), \quad (3)$$

where $\mathbf{u}$, ρ and μ are the macroscopic velocity, density and dynamic viscosity respectively; $\delta_t = 1$ is the time step; $f_\alpha^{(eq)}$ and $g_\alpha^{(eq)}$ are the corresponding equilibrium states of f_α and g_α, given by

$$f_\alpha^{(eq)}(\mathbf{x},t) = H_\alpha\phi + F_\alpha\left[p_0 - k\phi\nabla^2\phi - \frac{k}{6}|\nabla\phi|^2\right] + 3\omega_\alpha\phi(\mathbf{e}'_\alpha\cdot\mathbf{u}) + \omega_\alpha k\mathbf{e}'_\alpha\cdot\mathbf{G}(\phi)\cdot\mathbf{e}_\alpha, \quad (4)$$

$$\begin{aligned} g_\alpha^{(eq)}(\mathbf{x},t) = {} & \omega_\alpha\left[1 + 3(\mathbf{e}'_\alpha\cdot\mathbf{u}) + \frac{9}{2}(\mathbf{e}'_\alpha\cdot\mathbf{u})^2 - \frac{3}{2}\mathbf{u}^2 + \frac{3}{4}\mathbf{e}'_\alpha\cdot(\nabla\mathbf{u}+\mathbf{u}\nabla)\cdot\mathbf{e}_\alpha\right] \\ & + \omega_\alpha\frac{k}{\rho}\mathbf{e}'_\alpha\cdot\mathbf{G}(\phi)\cdot\mathbf{e}_\alpha - \frac{2}{3}F_\alpha\frac{k}{\rho}|\nabla\phi|^2 + 3\omega_\alpha\frac{1}{\rho}\nabla\cdot[\mu(\nabla\mathbf{u}+\mathbf{u}\nabla)]\cdot\mathbf{e}_\alpha \end{aligned}, \quad (5)$$

where

$$\omega_\alpha = \begin{cases} 2/9, & \\ 1/9, & \\ 1/72, & \end{cases} \quad F_\alpha = \begin{cases} -7/3, & \alpha = 0 \\ 1/3, & \alpha = 1,...,6 \\ 1/24, & \alpha = 7,...,14 \end{cases}, \quad (6\text{-}1)$$

$$H_\alpha = \begin{cases} 1, & \alpha = 0 \\ & \\ 0, & \alpha = 1,...,14 \end{cases}, \quad (6\text{-}2)$$

and

$$\mathbf{G}(\phi) = \frac{9}{2}(\nabla\phi)(\phi\nabla) - \frac{3}{2}|\nabla\phi|^2\mathbf{I}, \quad (7)$$

where, k is a constant parameter for determining the width of interface and the strength of surface tension. Given that $\psi(\phi)$ is the bulk free-energy density, then

$$p_0 = \phi\frac{\partial\psi}{\partial\phi} - \psi. \quad (8)$$

The macroscopic quantities, $\mathbf{u}^*$, ϕ, ρ, μ can be evaluated as

$$\phi = \sum_\alpha f_\alpha, \quad \mathbf{u}^* = \sum_\alpha \mathbf{e}_\alpha g_\alpha, \quad (9)$$

$$\mu = \frac{\rho - \rho_G}{\rho_L - \rho_G}(\mu_L - \mu_G) + \mu_G, \quad (10)$$

$$\rho = \begin{cases} \rho_G, & \phi < \phi_G \\ \dfrac{\phi - \phi_G}{\phi_L - \phi_G}(\rho_L - \rho_G) + \rho_G, & \phi_G \le \phi \le \phi_L \\ \rho_L, & \phi > \phi_L \end{cases}, \quad (11)$$

where the subscript *L* and *G* stand for liquid and gas respectively.

To obtain the velocity field which satisfies the continuity equation ($\nabla\cdot\mathbf{u} = 0$), $\mathbf{u}^*$ is corrected by following equations:

$$\mathbf{u} - \mathbf{u}^* = -\frac{\nabla p}{\rho}, \quad (12)$$

$$\nabla \cdot \mathbf{u}^* = \nabla \cdot \left(\frac{\nabla p}{\rho} \right) \ , \qquad (13)$$

where p is the pressure of the two-phase fluid, which can be obtained by solving Eq. (13) in the following LBM framework,

$$h_\alpha (\mathbf{x} + \mathbf{e}_\alpha, n+1) = h_\alpha (\mathbf{x}, n) - \frac{1}{\tau}[h_\alpha (\mathbf{x}, n) - \omega_\alpha p(\mathbf{x}, n)] - \frac{\omega_\alpha}{3} \frac{1}{\rho} \nabla \cdot \mathbf{u}^*, \quad (14)$$

where, n is the number of iterations and $\tau = 0.5 + 1/\rho$ is the relaxation time. The pressure at step $n+1$ is given by

$$p(\mathbf{x}, n+1) = \sum_\alpha h_\alpha (\mathbf{x}, n+1) . \qquad (15)$$

The convergent pressure p is determined when for whole computational domain V

$$\forall \mathbf{x} \in V, \ | p(\mathbf{x}, n+1) - p(\mathbf{x}, n+1) | < \varepsilon \ . \qquad (16)$$

2.2. Partial wetting boundary

To implement the wetting boundary condition, here a Landau free energy function (Briant et al., 2004; Briant and Yeomans, 2004) is introduced as

$$\Psi = \int_V dV [\psi(\phi) + k(\nabla \phi)^2 / 2] \ . \qquad (17)$$

For an isothermal system, assuming the free energy density $\psi(\phi)$ takes the following simple form particularly as (Jamet et al., 2001)

$$\psi(\phi) = \beta (\phi - \phi_G)^2 (\phi - \phi_L)^2 + \mu_b \phi - p_b \ , (18)$$

where, β is the constant relating to interfacial thickness.

By substitution of Eq. (18), Eq. (8) becomes

$$p_0 = \beta (\phi - \phi_L)(\phi - \phi_G) (3\phi^2 - \phi\phi_L - \phi\phi_G - \phi_L \phi_G) + p_b \ . \qquad (19)$$

In a plane interface under an equilibrium condition, the density profile across the interface on equilibrium is represented as

$$\phi(z) = \frac{\phi_L + \phi_G}{2} + \frac{\phi_L - \phi_G}{2} \tanh\left(\frac{2z}{D} \right), \qquad (20)$$

where z is the coordinate normal to the interface; the interface thickness D is given by

$$D = \frac{4}{\phi_L - \phi_G} \sqrt{\frac{k}{2\beta}} \ . \qquad (21)$$

The fluid-fluid (liquid-gas) surface tension force σ_{LG} is expressed as (Rowlinson and Widom, 1989)

$$\sigma_{LG} = \frac{(\phi_L - \phi_G)^3}{6} \sqrt{2k\beta} \ . \qquad (22)$$

According to the Young's law (Young, 1805), when a liquid-gas interface meets a partial wetting solid wall, the contact angle, θ_w, measured in the liquid, can be calculated from a balance of surface tension forces at the contact line as

$$\cos\theta_w = \frac{\sigma_{SG} - \sigma_{SL}}{\sigma_{LG}} \ , \qquad (23)$$

where σ_{SG} and σ_{SL} are the solid-gas and solid-liquid surface tension forces, respectively. To calculate the surface tension forces σ_{SG} and σ_{SL} within a mean field framework, Assuming that the fluid-solid interactions are sufficiently short-range such that they contribute a surface integral to the total free energy of the system (Cahn, 1977), the total free energy becomes

$$\Psi = \int_V dV [\psi(\phi) + k(\nabla \phi)^2 / 2] + \int_s dS \, \Phi(\phi_s) , (24)$$

where ϕ_s is the order parameter on the wall; S is the surface of volume V.

Considering a 1-Dimensional problem and remaining only the first-order term of power series expansion with respect to ϕ_s of

$\Phi(\phi_s)$, i.e. $\Phi(\phi_s) = -\lambda\phi_s$, Eq. (24) is reduced to

$$\Psi = \int_V dz[\psi(\phi) + k(d\phi/dz)^2/2] - \lambda\phi_s . \qquad (25)$$

Minimizing Eq. (25) by variational calculus subject to natural boundary conditions leads to two conditions as (Briant et al., 2002):

$$\frac{\partial\psi}{\partial\phi} - k\frac{d^2\phi}{dz^2} = \mu_b, \text{ for } z > 0; \qquad (26)$$

$$k\left(\frac{d\phi}{dz}\right) = \frac{d\Phi(\phi_s)}{d\phi_s} = -\lambda, \text{for } z = 0. \qquad (27)$$

A first integral for Eq. (26) yields,

$$\frac{k}{2}\left(\frac{d\phi}{dz}\right)^2 = \beta(\phi-\phi_G)^2(\phi-\phi_L)^2 = W(\phi). \qquad (28)$$

Then ϕ_s can be determined by substituting Eq. (28) into Eq. (27) and be written as

$$-\lambda = \pm\sqrt{2kW(\phi_s)} \quad . \qquad (29)$$

The surface tension between wall and fluid, σ_{SF}, is given by

$$\sigma_{SF} = -\lambda\phi_s + \int\sqrt{2kW}\,d\phi . \qquad (30)$$

Given that wetting potential

$$\Omega = \frac{4\lambda}{(\phi_L-\phi_G)^2\sqrt{2k\beta}} . \qquad (31)$$

The following expressions for surface tensions are obtained:

$$\sigma_{SG} = -\lambda\frac{\phi_L+\phi_G}{2} + \frac{\sigma_{LG}}{2} - \frac{\sigma_{LG}}{2}(1-\Omega)^{3/2}, \qquad (32)$$

$$\sigma_{SL} = -\lambda\frac{\phi_L+\phi_G}{2} + \frac{\sigma_{LG}}{2} - \frac{\sigma_{LG}}{2}(1+\Omega)^{3/2}. \qquad (33)$$

The wetting angle is determined by substituting Eq. (22) and Eqs. (32) and (33) into Eq. (23) and written as

$$\cos\theta_w = \frac{(1+\Omega)^{3/2} - (1-\Omega)^{3/2}}{2} \quad . \qquad (34)$$

For a given wetting angle in the range of $0 < \theta_w < \pi$, Ω can be obtained from Eq. (34) as

$$\Omega = 2\,\mathrm{sgn}\left(\frac{\pi}{2}-\theta_w\right)\left\{\cos\left(\frac{\gamma}{3}\right)\left[1-\cos\left(\frac{\gamma}{3}\right)\right]\right\}^{1/2}, \qquad (35)$$

where $\gamma = \arccos(\sin^2\theta_w)$ and $\mathrm{sgn}(\xi)$ gives the sign of ξ. It is noted from Eq. (35) that the required wetting potential Ω can be obtained by choosing a desired contact angle θ_w and then calculating λ by solving Eq. (31) with the newly obtained Ω.

3. Results and Discussions

The motion of water droplets at normal temperature surrounded by air on a partial wetting wall is considered. The gravitational force is taken into account by adding the term $-3\omega_\alpha e_{\alpha 3}(1-\rho_G/\rho)g$ to the right hand side of Eq. (3), where g is the dimensionless gravitational acceleration. The densities of two fluids are set at $\tilde{\rho}_L = 1\times10^3\, kgm^{-3}$ and $\tilde{\rho}_G = 1.29 kgm^{-3}$, and the viscosities of them are at $\tilde{\mu}_L = 1\times10^{-3}\, kgm^{-1}s^{-1}$ and $\tilde{\mu}_G = 1.935\times10^{-5}\, kgm^{-1}s^{-1}$, respectively. The initial surface tension between water and air is of $\tilde{\sigma}_{LG} = 1\times10^{-3}\, kgs^{-2}$ and the gravitational acceleration is set at $\tilde{g} = 9.8 ms^{-2}$. To relate the physical parameters with simulation parameters, a length scale of $L_0 = 1\times10^{-4} m$, time scale of $T_0 = 1\times10^{-6} s$ and mass scale of $M_0 = 1\times10^{-12} kg$ are chosen; these lead to the dimensionless parameters: $\rho_L = 1\times10^3$; $\rho_G = 1.29$; $\mu_L = 0.1$; $\mu_G = 1.935\times10^{-3}$; $\phi_L = 0.4$; $\phi_G = 0.1$; $k = 0.05$; and $g = 9.8\times10^{-8}$. Unless otherwise specified, the flowing simulations are within a cuboid

computational domain with a no-slip boundary at the lower surface .i.e. the flat partial wetting wall and the free outflow/inflow boundaries at the other five surfaces. ε in Eq. (16) is set as $\varepsilon = 1\times10^{-6}$.

As a check on consistency of theoretical prediction and present numerical results, the method is firstly applied to the problems of a water droplet spreading on uniform wetting surfaces. Initially, the shape of droplet is spherical, the distance between the centre of the sphere and the wall is of $r = 1\times10^{-3}m$, where r is the radius of the initial droplet. Fig. 2 shows the equilibrium interfacial shapes at $x = L_x/2$ under initial conditions of $\theta_w = \pi/4$ and $\theta_w = \pi/2$, respectively. Where, Fig.2 (a) and (b) show the equilibrium droplet shapes obtained at $t = 0.0675s$ and $t = 0.0415s$ respectively. By measuring the obtained equilibrium contact angles, it is noted that the results of the simulation agree well with those of initial prediction, i.e. $\theta_w = \pi/4$ for the dashed line interface and $\theta_w = \pi/2$ for the solid line interface. This indicates that the present LBM can be used as a reliable way to study fluidic control of wetting related subjects.

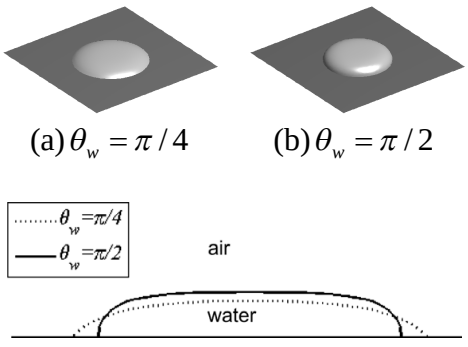

(c) Comparison in 2D view

Fig. 2: Equilibrium interfacial shapes.

In the present method, both velocities and pressures are corrected by solving an additional Poisson equation after each collision-stream step. Such corrections are able to make the velocity field to satisfy the continuity equation and to smooth the pressure distribution across the interface, so that to ensure the numerical stability. In Fig. 3, a velocity field on the cross section of $x = L_x/2$ at t=0.006s under initial conditions of $\theta_w = \pi/4$, where the solid line is the interface between two phases, is given to show that the present method can obtain a stable and reasonable velocity distribution.

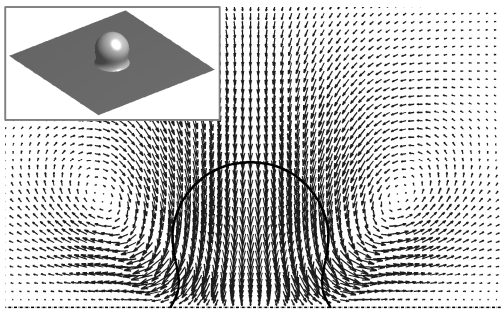

Fig. 3: Velocity distribution on the cross section, $\theta_w = \pi/4$, t=0.006s.

Fig. 4 shows how a small hemispherical water droplet evolves with time on a heterogeneous surface. A narrow hydrophobic strip with width of $l = 6\times10^{-4}m$ is located at the centreline of the surface where $\theta_w = 5\pi/6$, and the other areas are occupied by the hydrophilic surface with $\theta_w = \pi/6$. The initial droplet which has a radius $r = 1.5\times10^{-3}m$ is set at the centre of the wetting surface. As shown in the figure, the droplet stretches over the area occupied by the hydrophilic surface in the early stages of flow evolution due to the adhesive force of the surface. At the same time, the droplet rapidly contracts inward along the hydrophobic strip. With the development of time, the droplet spreads further on the hydrophilic area, and meanwhile contracts inward along the hydrophobic strip and finally breaks up into two smaller droplets. The newly formed droplets continue spreading until an equilibrium state is reached.

To define a cross section perpendicular to the centreline of the hydrophobic strip, Fig. 5 shows the evaluation of the interface and the corresponding velocity fields there.

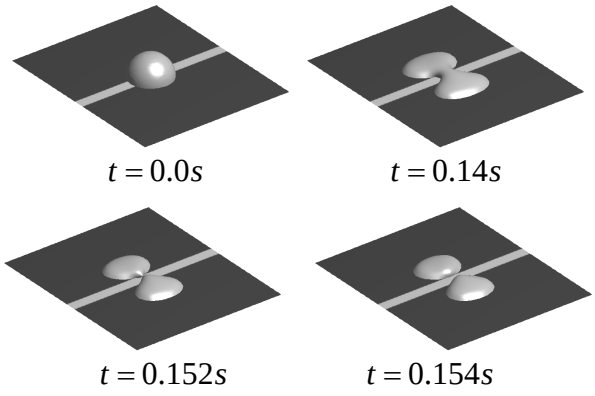

Fig. 4: Snapshots of a droplet spreading on a surface with a hydrophobic strip.

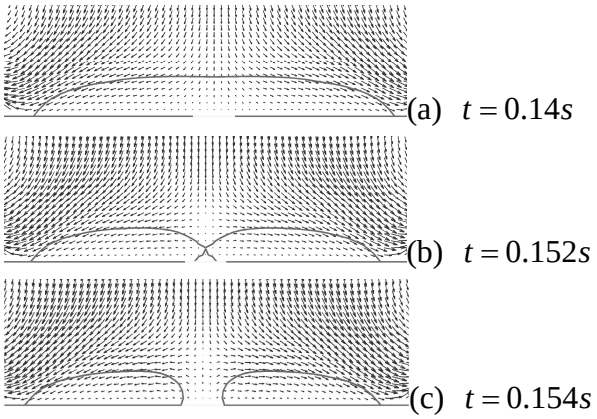

Fig. 5: Evolution of the interface and the corresponding velocity fields.

Then, a single droplet spreading on a heterogeneous surface with intersecting hydrophobic strips is simulated. As shown in Fig. 6, two cross hydrophobic strips ($\theta_w = 5\pi/9$) with width of $l = 9\times10^{-4}m$ are located at the centreline of the square surface, the other areas are occupied by the hydrophilic surface with $\theta_w = \pi/4$. Initially, the droplet has a shape of spherical cap with radius of $r = 2\times10^{-3}m$ and height of $h = 1\times10^{-3}m$, and is set at the centre of the surface. The shape evolution of the droplet with time is shown in Fig. 6. From the figure, it can be seen that the droplet symmetrically spreads into four hydrophilic sections with the development of time and finally reaches an equilibrium state with a shape of four-leaved flower.

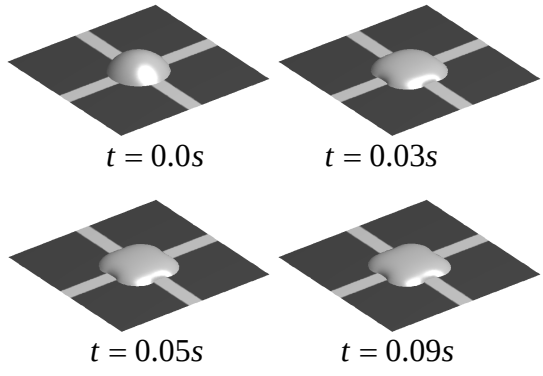

Fig. 6: Snapshots of a droplet spreading on a surface with intersecting hydrophobic strips.

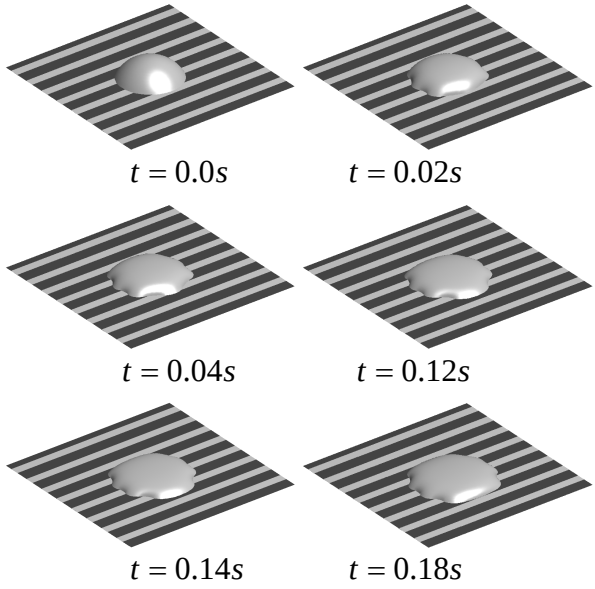

Fig. 7: Droplet spreading on a surface consisting of alternating and parallel strips.

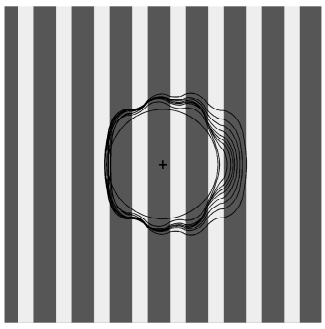

Fig. 8: Evolution of moving contact line on a surface with alternating and parallel strips.

Finally, the evolution of a water droplet spreading on the heterogeneous surface

consisting of alternating and parallel hydrophilic strips with the width and the steady-state contact angle of $l = 7\times10^{-4}m$, $\theta_w = 2\pi/9$ and the hydrophobic strips with $l = 5\times10^{-4}m$ and $\theta_w = 5\pi/9$ is considered. Initially, the droplet has a shape of spherical cap with radius $r = 2\times10^{-3}m$ and height $h = 1\times10^{-3}m$; the centre of initial circular contact line is set on the hydrophilic surface and the minimum distances form it to two neighbouring hydrophobic strips are $2\times10^{-4}m$ and $5\times10^{-4}m$ respectively. The behaviour of 3D droplet and the time evolution of the contact are shown in Figs. 7 and 8 respectively. It can be noted from the figures that, the droplet can finally reach a symmetric shape although the centre of the droplet is initially set at a location other than the centreline of any strip.

As shown in Fig. 9, two cross sections, CS-I and CS-II, vertical to the heterogeneous surface are defined. L1 and L2 show the corresponding lines of intersection of CS-I and CS-II with the heterogeneous surface respectively.

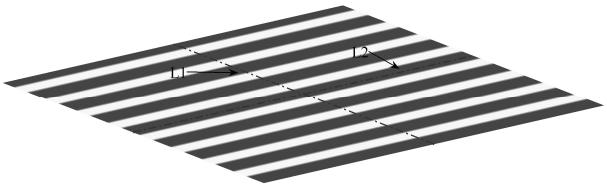

Fig. 9: Definition of L1 and L2

Fig. 10 and 11 show the evolution of the interface and the corresponding velocity fields on cross section CS-I and CS-II respectively. From Fig. 10, it can be found that the droplet moves to the left. This should be caused by the asymmetry of the wall surface tension with respect to the centre line of the droplet. As shown in Fig. 9, the hydrophilic area occupied by the droplet at the left side of L2 is larger then that at the right side of L2. This means that the wall total surface tension at the left part of the droplet is larger than right one. Therefore, the droplet tents to reach a steady state when the centre of the droplet reaches a centreline of any strip if the heterogeneous surface is horizontal. See Fig. 11, the cross section connects with the hydrophilic strip of the surface. So, the contact angle is less then 90 degree. Also, the interface and velocity field are symmetric due to the symmetry of the surface tension distribution.

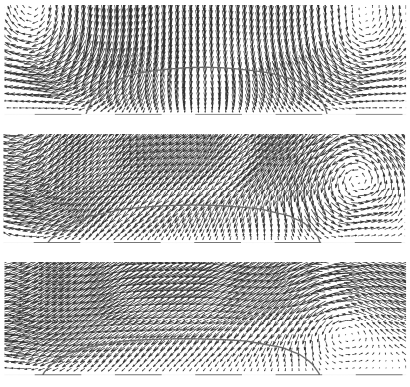

(a) $t = 0.02s$

(b) $t = 0.12s$

(c) $t = 0.14s$

Fig. 10: Evolution of interface and the corresponding velocity fields on CS-I.

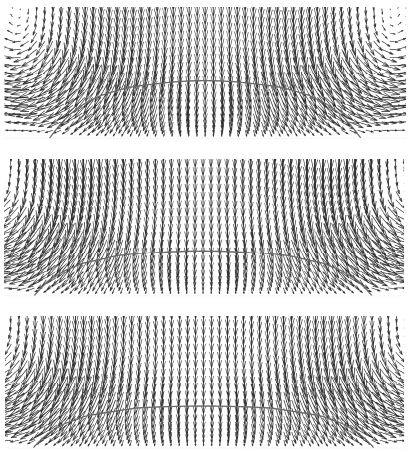

(a) $t = 0.02s$

(b) $t = 0.12s$

(c) $t = 0.14s$

Fig. 11: Evolution of the interface and the corresponding velocity fields on CS-II.

4. Conclusions

In this paper, a lattice Boltzmann method for calculating liquid droplet behaviours on particle wetting surfaces typically for the system of liquid-gas of a large density ratio has been reported. The method has developed a novel treatment for partial wetting boundaries which existing when a liquid droplet spreads on a partial wetting surface. In the present study, a water droplet in air spreading on partial wetting surface are studied and simulated based on the current

LBM scheme. To check the reliability of the scheme, the method is firstly applied to the problems of a water droplet spreading on the uniform wetting surface with different contact angles. By measuring the obtained equilibrium contact angles, it is noted that the results of the simulation agree well with those of initial prediction, which indicate that the present LBM can be used as a reliable way to study the interaction between the two-phase flow and wetting surfaces. Then, using the method, water droplets on three types of heterogeneous surfaces are studied. One is the a heterogeneous wetting wall which combines a narrow hydrophobic strip; the other is a wetting surface combined with cross hydrophobic strips; the third case is concerned with the heterogeneous surface consisting of alternating and parallel hydrophilic strips. The interactions between the fluid-fluid interface and the partial wetting wall are typically considered in the simulations. The droplet dynamics on partial wetting surfaces including the phenomena of droplet spreading, breaking up and also the migration of the centre caused by asymmetrical wall surface tension have been analyzed. And the corresponding mechanisms have been studied on the basis of the obtained evolutions of phase distribution and flow fields.

Acknowledgement

This work is supported by the UK EPSRC under grant EP/D500125/1.

References

Briant, A. J., et al., 2002. Lattice Boltzmann simulations of contact line motion in a liquid-gas system. Phil. Trans. R. Soc. Lond. A. 360**,** 485-495.

Briant, A. J., et al., 2004. Lattice Boltzmann simulations of contact line motion. I. Liquid-gas systems. Phys. Rev. E. 69**,** 031602.

Briant, A. J., Yeomans, J. M., 2004. Lattice Boltzmann simulations of contact line motion. II. Binary fluids. Phys. Rev. E. 69**,** 031603.

Cahn, J. W., 1977. Critical-Point Wetting. J. Chem. Phys. 66**,** 3667-3672.

Chen, S., Doolen, G. D., 1998. Lattice Boltzmann method for fluid flows. Ann. Rev. Fluid Mech. 30**,** 329-364.

Dupuis, A., Yeomans, J. M., 2004. Lattice Boltzmann modelling of droplets on chemically heterogeneous surfaces. Future Gener. Comput. Syst. 20**,** 993-1001.

Dupuis, A., Yeomans, J. M., 2005. Modeling droplets on superhydrophobic surfaces: Equilibrium states and transitions. Langmuir. 21**,** 2624-2629.

Gunstensen, A. K., et al., 1991. Lattice Boltzmann Model of Immiscible Fluids. Phys. Rev. A. 43**,** 4320-4327.

He, X. Y., et al., 1999. A lattice Boltzmann scheme for incompressible multiphase flow and its application in simulation of Rayleigh-Taylor instability. J. Comput. Phys. 152**,** 642-663.

Inamuro, T., et al., 2004. A lattice Boltzmann method for incompressible two-phase flows with large density differences. J. Comput. Phys. 198**,** 628-644.

Jamet, D., et al., 2001. The second gradient theory: a tool for the direct numerical simulation of liquid-vapor flows with phase-change. Nucl. Eng. Des. 204**,** 155-166.

Kusumaatmaja, H., et al., 2006. Lattice Boltzmann simulations of drop dynamics. Math. Comput. Simul. 72**,** 160-164.

Rowlinson, J. S., Widom, B., 1989. Molecular Theory of Capillarity. Clarendon, Oxford.

Shan, X. W., Chen, H. D., 1993. Lattice Boltzmann Model for Simulating Flows with Multiple Phases and Components. Phys. Rev. E. 47**,** 1815-1819.

Swift, M. R., et al., 1996. Lattice Boltzmann simulations of liquid-gas and binary fluid systems. Phys. Rev. E. 54**,** 5041-5052.

Swift, M. R., et al., 1995. Lattice Boltzmann Simulation of Nonideal Fluids. Phys. Rev. Lett. 75**,** 830-833.

Yan, Y.Y., Zu, Y.Q., 2007. *J. Computational Physics*, 227 (1), 763-775.

Young, T., 1805. An essay on the cohesion of fluids. Phi. Trans. R. Soc. Lond. . 95**,** 65-87.